Transverse single-spin asymmetries of midrapidity π0 and η mesons in polarized p+p collisions at √s=200 GeV

(PHENIX Collaboration) Acharya, U. A.; Aidala, C.; Akiba, Y.; Alfred, M.; Andrieux, V.; Apadula, N.; Asano, H.; Azmoun, B.; Babintsev, V.; Bandara, N. S.; ...

Source / Izvornik: **Physical Review D, 2021, 103**

Journal article, Published version
Rad u časopisu, Objavljena verzija rada (izdavačev PDF)

https://doi.org/10.1103/PhysRevD.103.052009

Permanent link / Trajna poveznica: https://urn.nsk.hr/urn:nbn:hr:217:016521

Transverse single-spin asymmetries of midrapidity π^0 and η mesons in polarized $p+p$ collisions at $\sqrt{s}=200$ GeV

U. A. Acharya,[20] C. Aidala,[40] Y. Akiba,[53,54,†] M. Alfred,[22] V. Andrieux,[40] N. Apadula,[27] H. Asano,[33,53] B. Azmoun,[7] V. Babintsev,[23] N. S. Bandara,[39] K. N. Barish,[8] S. Bathe,[5,54] A. Bazilevsky,[7] M. Beaumier,[8] R. Belmont,[11,46] A. Berdnikov,[56] Y. Berdnikov,[56] L. Bichon,[63] B. Blankenship,[63] D. S. Blau,[32,43] J. S. Bok,[45] V. Borisov,[56] M. L. Brooks,[35] J. Bryslawskyj,[5,8] V. Bumazhnov,[23] S. Campbell,[12] V. Canoa Roman,[59] R. Cervantes,[59] C. Y. Chi,[12] M. Chiu,[7] I. J. Choi,[24] J. B. Choi,[29,*] Z. Citron,[64] M. Connors,[20,54] R. Corliss,[59] N. Cronin,[59] M. Csanád,[15] T. Csörgő,[16,65] T. W. Danley,[47] M. S. Daugherity,[1] G. David,[7,59] K. DeBlasio,[44] K. Dehmelt,[59] A. Denisov,[23] A. Deshpande,[54,59] E. J. Desmond,[7] A. Dion,[59] D. Dixit,[59] J. H. Do,[66] A. Drees,[59] K. A. Drees,[6] J. M. Durham,[35] A. Durum,[23] A. Enokizono,[53,55] H. En'yo,[53] R. Esha,[59] S. Esumi,[62] B. Fadem,[41] W. Fan,[59] N. Feege,[59] D. E. Fields,[44] M. Finger,[9] M. Finger, Jr.,[9] D. Firak,[14] D. Fitzgerald,[40] S. L. Fokin,[32] J. E. Frantz,[47] A. Franz,[7] A. D. Frawley,[19] Y. Fukuda,[62] C. Gal,[59] P. Gallus,[13] P. Garg,[3,59] H. Ge,[59] M. Giles,[59] F. Giordano,[24] Y. Goto,[53,54] N. Grau,[2] S. V. Greene,[63] M. Grosse Perdekamp,[24] T. Gunji,[10] H. Guragain,[20] T. Hachiya,[42,53,54] J. S. Haggerty,[7] K. I. Hahn,[17] H. Hamagaki,[10] H. F. Hamilton,[1] S. Y. Han,[17,31] J. Hanks,[59] S. Hasegawa,[28] T. O. S. Haseler,[20] X. He,[20] T. K. Hemmick,[59] J. C. Hill,[27] K. Hill,[11] A. Hodges,[20] R. S. Hollis,[8] K. Homma,[21] B. Hong,[31] T. Hoshino,[21] N. Hotvedt,[27] J. Huang,[7] S. Huang,[63] K. Imai,[28] M. Inaba,[62] A. Iordanova,[8] D. Isenhower,[1] D. Ivanishchev,[51] B. V. Jacak,[59] M. Jezghani,[20] Z. Ji,[59] X. Jiang,[35] B. M. Johnson,[7,20] D. Jouan,[49] D. S. Jumper,[24] J. H. Kang,[66] D. Kapukchyan,[8] S. Karthas,[59] D. Kawall,[39] A. V. Kazantsev,[32] V. Khachatryan,[59] A. Khanzadeev,[51] A. Khatiwada,[35] C. Kim,[8,31] E.-J. Kim,[29] M. Kim,[57] D. Kincses,[15] A. Kingan,[59] E. Kistenev,[7] J. Klatsky,[19] P. Kline,[59] T. Koblesky,[11] D. Kotov,[51,56] S. Kudo,[62] B. Kurgyis,[15] K. Kurita,[55] Y. Kwon,[66] J. G. Lajoie,[27] D. Larionova,[56] M. Larionova,[56] A. Lebedev,[27] S. Lee,[66] S. H. Lee,[27,40,59] M. J. Leitch,[35] Y. H. Leung,[59] N. A. Lewis,[40] X. Li,[35] S. H. Lim,[35,52,66] M. X. Liu,[35] V.-R. Loggins,[24] S. Lökös,[15] K. Lovasz,[14] D. Lynch,[7] T. Majoros,[14] Y. I. Makdisi,[6] M. Makek,[67] V. I. Manko,[32] E. Mannel,[7] M. McCumber,[35] P. L. McGaughey,[35] D. McGlinchey,[11,35] C. McKinney,[24] M. Mendoza,[8] W. J. Metzger,[16] A. C. Mignerey,[38] A. Milov,[64] D. K. Mishra,[4] J. T. Mitchell,[7] Iu. Mitrankov,[56] G. Mitsuka,[30,54] S. Miyasaka,[53,61] S. Mizuno,[53,62] M. M. Mondal,[59] P. Montuenga,[24] T. Moon,[31,66] D. P. Morrison,[7] S. I. Morrow,[63] B. Mulilo,[31,53] T. Murakami,[33,53] J. Murata,[53,55] K. Nagai,[61] K. Nagashima,[21] T. Nagashima,[55] J. L. Nagle,[11] M. I. Nagy,[15] I. Nakagawa,[53,54] K. Nakano,[53,61] C. Nattrass,[60] S. Nelson,[18] T. Niida,[62] R. Nouicer,[7,54] T. Novák,[16,65] N. Novitzky,[59,62] A. S. Nyanin,[32] E. O'Brien,[7] C. A. Ogilvie,[27] J. D. Orjuela Koop,[11] J. D. Osborn,[40,48] A. Oskarsson,[36] G. J. Ottino,[44] K. Ozawa,[30,62] V. Pantuev,[25] V. Papavassiliou,[45] J. S. Park,[57] S. Park,[53,57,59] S. F. Pate,[45] M. Patel,[27] W. Peng,[63] D. V. Perepelitsa,[7,11] G. D. N. Perera,[45] D. Yu. Peressounko,[32] C. E. PerezLara,[59] J. Perry,[27] R. Petti,[7] M. Phipps,[7,24] C. Pinkenburg,[7] R. P. Pisani,[7] M. Potekhin,[7] A. Pun,[47] M. L. Purschke,[7] P. V. Radzevich,[56] N. Ramasubramanian,[59] K. F. Read,[48,60] D. Reynolds,[58] V. Riabov,[43,51] Y. Riabov,[51,56] D. Richford,[5] T. Rinn,[24,27] S. D. Rolnick,[8] M. Rosati,[27] Z. Rowan,[5] J. Runchey,[27] A. S. Safonov,[56] T. Sakaguchi,[7] H. Sako,[28] V. Samsonov,[43,51] M. Sarsour,[20] S. Sato,[28] B. Schaefer,[63] B. K. Schmoll,[60] K. Sedgwick,[8] R. Seidl,[53,54] A. Sen,[27,60] R. Seto,[8] A. Sexton,[38] D. Sharma,[59] D. Sharma,[59] I. Shein,[23] T.-A. Shibata,[53,61] K. Shigaki,[21] M. Shimomura,[27,42] T. Shioya,[62] P. Shukla,[4] A. Sickles,[24] C. L. Silva,[35] D. Silvermyr,[36] B. K. Singh,[3] C. P. Singh,[3] V. Singh,[3] M. Slunečka,[9] K. L. Smith,[19] M. Snowball,[35] R. A. Soltz,[34] W. E. Sondheim,[35] S. P. Sorensen,[60] I. V. Sourikova,[7] P. W. Stankus,[48] S. P. Stoll,[7] T. Sugitate,[21] A. Sukhanov,[7] T. Sumita,[53] J. Sun,[59] X. Sun,[20] Z. Sun,[14] J. Sziklai,[65] K. Tanida,[28,54,57] M. J. Tannenbaum,[7] S. Tarafdar,[63,64] G. Tarnai,[14] R. Tieulent,[20,37] A. Timilsina,[27] T. Todoroki,[54,62] M. Tomášek,[13] C. L. Towell,[1] R. S. Towell,[1] I. Tserruya,[64] Y. Ueda,[21] B. Ujvari,[14] H. W. van Hecke,[35] J. Velkovska,[63] M. Virius,[13] V. Vrba,[13,26] N. Vukman,[67] X. R. Wang,[45,54] Y. S. Watanabe,[10] C. P. Wong,[20,35] C. L. Woody,[7] Y. Wu,[8] C. Xu,[45] Q. Xu,[63] L. Xue,[20] S. Yalcin,[59] Y. L. Yamaguchi,[59] H. Yamamoto,[62] A. Yanovich,[23] J. H. Yoo,[31] I. Yoon,[57] H. Yu,[45,50] I. E. Yushmanov,[32] W. A. Zajc,[12] A. Zelenski,[6] Y. Zhai,[27] S. Zharko,[56] and L. Zou[8]

(PHENIX Collaboration)

[1]*Abilene Christian University, Abilene, Texas 79699, USA*
[2]*Department of Physics, Augustana University, Sioux Falls, South Dakota 57197, USA*
[3]*Department of Physics, Banaras Hindu University, Varanasi 221005, India*
[4]*Bhabha Atomic Research Centre, Bombay 400 085, India*
[5]*Baruch College, City University of New York, New York, New York 10010, USA*
[6]*Collider-Accelerator Department, Brookhaven National Laboratory, Upton, New York 11973-5000, USA*
[7]*Physics Department, Brookhaven National Laboratory, Upton, New York 11973-5000, USA*
[8]*University of California-Riverside, Riverside, California 92521, USA*
[9]*Charles University, Ovocný trh 5, Praha 1, 116 36, Prague, Czech Republic*

[10]*Center for Nuclear Study, Graduate School of Science, University of Tokyo, 7-3-1 Hongo, Bunkyo, Tokyo 113-0033, Japan*
[11]*University of Colorado, Boulder, Colorado 80309, USA*
[12]*Columbia University, New York, New York 10027, USA, and Nevis Laboratories, Irvington, New York 10533, USA*
[13]*Czech Technical University, Zikova 4, 166 36 Prague 6, Czech Republic*
[14]*Debrecen University, H-4010 Debrecen, Egyetem tér 1, Hungary*
[15]*ELTE, Eötvös Loránd University, H-1117 Budapest, Pázmány P. s. 1/A, Hungary*
[16]*Eszterházy Károly University, Károly Róbert Campus, H-3200 Gyöngyös, Mátrai út 36, Hungary*
[17]*Ewha Womans University, Seoul 120-750, Korea*
[18]*Florida A&M University, Tallahassee, Florida 32307, USA*
[19]*Florida State University, Tallahassee, Florida 32306, USA*
[20]*Georgia State University, Atlanta, Georgia 30303, USA*
[21]*Hiroshima University, Kagamiyama, Higashi-Hiroshima 739-8526, Japan*
[22]*Department of Physics and Astronomy, Howard University, Washington, D.C. 20059, USA*
[23]*IHEP Protvino, State Research Center of Russian Federation, Institute for High Energy Physics, Protvino, 142281, Russia*
[24]*University of Illinois at Urbana-Champaign, Urbana, Illinois 61801, USA*
[25]*Institute for Nuclear Research of the Russian Academy of Sciences, prospekt 60-letiya Oktyabrya 7a, Moscow 117312, Russia*
[26]*Institute of Physics, Academy of Sciences of the Czech Republic, Na Slovance 2, 182 21 Prague 8, Czech Republic*
[27]*Iowa State University, Ames, Iowa 50011, USA*
[28]*Advanced Science Research Center, Japan Atomic Energy Agency, 2-4 Shirakata Shirane, Tokai-mura, Naka-gun, Ibaraki-ken 319-1195, Japan*
[29]*Jeonbuk National University, Jeonju, 54896, Korea*
[30]*KEK, High Energy Accelerator Research Organization, Tsukuba, Ibaraki 305-0801, Japan*
[31]*Korea University, Seoul 02841, Korea*
[32]*National Research Center "Kurchatov Institute," Moscow, 123098, Russia*
[33]*Kyoto University, Kyoto 606-8502, Japan*
[34]*Lawrence Livermore National Laboratory, Livermore, California 94550, USA*
[35]*Los Alamos National Laboratory, Los Alamos, New Mexico 87545, USA*
[36]*Department of Physics, Lund University, Box 118, SE-221 00 Lund, Sweden*
[37]*IPNL, CNRS/IN2P3, Université Lyon, Université Lyon 1, F-69622, Villeurbanne, France*
[38]*University of Maryland, College Park, Maryland 20742, USA*
[39]*Department of Physics, University of Massachusetts, Amherst, Massachusetts 01003-9337, USA*
[40]*Department of Physics, University of Michigan, Ann Arbor, Michigan 48109-1040, USA*
[41]*Muhlenberg College, Allentown, Pennsylvania 18104-5586, USA*
[42]*Nara Women's University, Kita-uoya Nishi-machi Nara 630-8506, Japan*
[43]*National Research Nuclear University, MEPhI, Moscow Engineering Physics Institute, Moscow, 115409, Russia*
[44]*University of New Mexico, Albuquerque, New Mexico 87131, USA*
[45]*New Mexico State University, Las Cruces, New Mexico 88003, USA*
[46]*Physics and Astronomy Department, University of North Carolina at Greensboro, Greensboro, North Carolina 27412, USA*
[47]*Department of Physics and Astronomy, Ohio University, Athens, Ohio 45701, USA*
[48]*Oak Ridge National Laboratory, Oak Ridge, Tennessee 37831, USA*
[49]*IPN-Orsay, Université Paris-Sud, CNRS/IN2P3, Université Paris-Saclay, BP1, F-91406, Orsay, France*
[50]*Peking University, Beijing 100871, People's Republic of China*
[51]*PNPI, Petersburg Nuclear Physics Institute, Gatchina, Leningrad region, 188300, Russia*
[52]*Pusan National University, Pusan 46241, Korea*
[53]*RIKEN Nishina Center for Accelerator-Based Science, Wako, Saitama 351-0198, Japan*
[54]*RIKEN BNL Research Center, Brookhaven National Laboratory, Upton, New York 11973-5000, USA*
[55]*Physics Department, Rikkyo University, 3-34-1 Nishi-Ikebukuro, Toshima, Tokyo 171-8501, Japan*
[56]*Saint Petersburg State Polytechnic University, St. Petersburg, 195251, Russia*
[57]*Department of Physics and Astronomy, Seoul National University, Seoul 151-742, Korea*
[58]*Chemistry Department, Stony Brook University, SUNY, Stony Brook, New York 11794-3400, USA*
[59]*Department of Physics and Astronomy, Stony Brook University, SUNY, Stony Brook, New York 11794-3800, USA*
[60]*University of Tennessee, Knoxville, Tennessee 37996, USA*

[61]Department of Physics, Tokyo Institute of Technology, Oh-okayama, Meguro, Tokyo 152-8551, Japan
[62]Tomonaga Center for the History of the Universe, University of Tsukuba, Tsukuba, Ibaraki 305, Japan
[63]Vanderbilt University, Nashville, Tennessee 37235, USA
[64]Weizmann Institute, Rehovot 76100, Israel
[65]Institute for Particle and Nuclear Physics, Wigner Research Centre for Physics, Hungarian Academy of Sciences (Wigner RCP, RMKI) H-1525 Budapest 114, P.O. Box 49, Budapest, Hungary
[66]Yonsei University, IPAP, Seoul 120-749, Korea
[67]Department of Physics, Faculty of Science, University of Zagreb, Bijenička c. 32 HR-10002 Zagreb, Croatia

(Received 30 November 2020; accepted 16 February 2021; published 22 March 2021)

We present a measurement of the transverse single-spin asymmetry for π^0 and η mesons in $p^\uparrow + p$ collisions in the pseudorapidity range $|\eta| < 0.35$ and at a center-of-mass energy of 200 GeV with the PHENIX detector at the Relativistic Heavy Ion Collider. In comparison with previous measurements in this kinematic region, these results have factor-of-3-smaller uncertainties. As hadrons, π^0 and η mesons are sensitive to both initial- and final-state nonperturbative effects for a mix of parton flavors. Comparisons of the differences in their transverse single-spin asymmetries have the potential to disentangle the possible effects of strangeness, isospin, or mass. These results can constrain the twist-3 trigluon collinear correlation function as well as the gluon Sivers function.

DOI: 10.1103/PhysRevD.103.052009

I. INTRODUCTION

Spin-momentum correlations in hadronic collisions have attracted increasing experimental and theoretical interest in the past two decades. In particular, transverse single-spin asymmetries (TSSAs) have been one of the primary means to probe transverse partonic dynamics in the nucleon. In the context of proton-proton collisions, one transversely polarized proton collides with another unpolarized proton and the TSSA measures the asymmetry in yields of particles that travel to the left versus the right of the polarized-proton-going direction. Large azimuthal asymmetries of up to ≈40% have been observed from transversely polarized $p^\uparrow + p$ collisions in light meson production at large Feynman-x ($x_F = 2p_L/\sqrt{s}$), from center of mass energies of ($\sqrt{s} = 4.9$ GeV) up to 500 GeV [1–6]. Next-to-leading order perturbative quantum chromodynamics (QCD) calculations that only include spin-momentum correlations from parton scattering predict small asymmetries on the order of m_q/Q [7], where m_q is the bare quark mass and Q is the hard scale, indicating that significant nonperturbative effects must dominate the large measured asymmetries. Two different approaches have been proposed to describe the large asymmetries observed in hadronic interactions.

In the first approach, nonperturbative parton distribution functions (PDFs) and fragmentation functions (FFs) are explicitly dependent on transverse momentum in the transverse-momentum-dependent (TMD) framework. These functions depend on a soft (k_T) and hard (Q) momentum scale such that $\Lambda_{\mathrm{QCD}} \lesssim k_T \ll Q$. One possible origin of the large TSSAs is the Sivers TMD PDF [8], which correlates the nucleon transverse spin with the parton transverse momentum, k_T. Another possible origin of the TSSA is the Collins TMD FF [9], which correlates the transverse polarization of a fragmenting quark to the angular distribution of hadrons.

The second approach to describe the large asymmetries relies on collinear higher-twist effects with multiparton correlations. In the twist-3 approach, interference arises between scattering amplitudes with one and two collinear partons, which leads to a nonzero TSSA. This approach applies to observables in which only one sufficiently hard momentum scale is measured, such that $Q \gg \Lambda_{\mathrm{QCD}}$ [10]. To keep the multiparton correlation functions process independent, the initial- and final-state interactions between the struck parton and the proton remnants are included in the hard perturbative part of the twist-3 collinear factorization [11]. Collinear twist-3 correlation functions are split into two types: the quark-gluon-quark functions (qgq) and the trigluon functions (ggg). In the context of initial-state effects, the qgq functions describe the interference from scattering off of one quark versus scattering off of a gluon and a quark of the same flavor, while the ggg functions capture the interference between scattering off of one gluon versus scattering off of two.

*Deceased.
†PHENIX Spokesperson: akiba@rcf.rhic.bnl.gov

The twist-3 approach is well suited to describe observed inclusive forward hadron asymmetries because the observed hadron p_T can be used as a proxy for the hard scale, and unlike the TMD approach, these correlation functions do not explicitly depend on a soft-scale transverse momentum. However, the twist-3 approach has been related to k_T moments of TMD PDFs and TMD FFs and has been shown to be equivalent to the TMD approach in the overlapping kinematic regime [12].

Because the Sivers function is odd under parity-and-time reversal (PT-odd, also referred to as "naïve T-odd"), to be nonzero it must include a soft-gluon exchange with the proton remnant. Depending on the process, the exchange can occur before and/or after the hard partonic scattering [13]. Significant nonzero asymmetries due to the Sivers TMD PDF have been measured in semi-inclusive deep-inelastic lepton-nucleon scattering (SIDIS) [14,15], where the soft-gluon exchange can only happen in the final state. In hadronic interactions where at least one final-state hadron is measured, both initial- and final-state interactions can play competing roles in the measured asymmetries; here TMD-factorization breaking has been predicted due to soft gluon exchanges that are possible in both the initial and final states simultaneously [16]. Additional leading-power spin asymmetries have been predicted in hadronic collisions due to this breakdown, without which these asymmetries would be subleading [17], but further work is needed to connect TMD-factorization breaking to experimentally measured asymmetries. Note that inclusive hadron TSSA measurements in hadronic collisions appear to plateau at p_T up to 5 GeV/c [3,5] and have been measured to be nonzero at up to $p_T \approx 7$ GeV/c [18]. Recent studies in the twist-3 framework have successfully described the p_T dependence of these forward asymmetries by including twist-3 effects in hadronization [19]. The twist-3 perturbative prediction is that the asymmetry should eventually decrease as the hard scale p_T continues increasing [17].

Since the inception of the collinear twist-3 and TMD factorization pictures, there has been theoretical evidence that they could combine to form a unified picture of TSSAs in hard processes. This concept was recently tested with the first simultaneous global analysis of TSSAs in SIDIS, Drell-Yan, e^+e^- annihilation, and proton-proton collisions [10]. This study used quark TMD PDFs and FFs to describe the asymmetries in processes that are sensitive to the soft-scale momentum, i.e., SIDIS, Drell-Yan, and e^+e^- annihilation. These TMD functions were also used to calculate collinear twist-3 qgq correlation functions which were applied to inclusive forward pion asymmetry measurements from the Relativistic Heavy Ion Collider (RHIC). This simultaneous description of TSSAs across multiple collision species indicates that all TSSAs have a common origin that is related to multiparton correlations.

Additional questions about the origin of the TSSAs in hadronic interactions remain. Forward jet measurements indicate that the TSSA is significantly smaller than neutral pion asymmetries at similar x_F and $\sqrt{s}$ [20]. Nonzero kaon and antiproton asymmetries observed at forward rapidities show that the measured asymmetries cannot be due only to proton valence quark contributions as naively predicted in a valencelike model, where the Sivers effect from sea quarks and/or gluons is ignored, and that the fragmentation of quarks into hadrons in which they are not valence quarks could play a role in the observed nonzero asymmetries [4,21]. Eta meson measurements, sensitive to potential effects from strange quark contributions, isospin, and/or hadron mass show forward asymmetries similar in magnitude to neutral pions [22]. At midrapidity at RHIC, nonzero TSSAs have been measured for charged pion pair production [23,24]. Even four decades after the initial discovery of large TSSAs in hadronic interactions [1], there remain many unresolved questions about their origin. Therefore it is crucial to continue extending measurements to try to better understand the nonperturbative dynamics which are responsible for the TSSAs in hadronic collisions.

In this paper we report a measurement of the TSSA of π^0 and η mesons in $p^\uparrow + p$ collisions at $\sqrt{s} = 200$ GeV in the midrapidity region $|\eta| < 0.35$. The data was taken during the 2015 RHIC run and a total integrated luminosity of approximately 60 pb^{-1} was collected. This measurement extends previous measurements from RHIC to higher p_T and reduces the statistical uncertainties by a factor of 3 in the overlapping p_T region.

II. ANALYSIS

The asymmetries are measured with transversely polarized proton beams where the average polarization of the clockwise beam was 0.58 ± 0.02 and that of the counterclockwise beam was 0.60 ± 0.02 [25]. The direction of the beam polarization was found to be consistent with the vertical within statistical uncertainties. The polarization direction of each beam independently changes bunch to bunch which reduces systematic uncertainties associated with variations in detector performance with time. The relative luminosity is the ratio of the integrated luminosity for bunches that were polarized in opposite directions. It is determined by the number of times each crossing fires a minimum-bias (MB) trigger and is measured to better than 10^{-4}. The relative luminosity values for both beams were limited to the range of 0.91 to 1.09 for all beam fills used in these measurements. The bunch-to-bunch changes in polarization direction also allow for polarization-averaged measurements and, for a single-spin asymmetry analysis, provide two ways to measure the TSSA with the same dataset. This is done by sorting the particle yields for the polarization directions of one beam at a time, effectively averaging over the polarization of the other beam. RHIC

uses eight different spin patterns for sequential fills which are carefully chosen to minimize potential effects from nonzero average polarization of either beam. The statistically independent asymmetries measured from the two beams are used to verify the analysis and are averaged together for the final result.

The data analysis procedure is similar to our previous measurements [5]. Neutral pion and eta mesons are reconstructed via their two-photon decays by using the midrapidity electromagnetic calorimeter (EMCal). The EMCal is located in two central arms, each covering $\Delta\phi = \pi/2$ in azimuth and $|\eta| < 0.35$ in pseudorapidity, centered at $\phi = \pi/16$ and $15\pi/16$. The EMCal comprises two different types of calorimeters: six sectors of sampling lead-scintillator calorimeters and two sectors of Čerenkov lead-glass calorimeters [26]. The two calorimeter systems have different granularity ($\delta\phi \times \delta\eta = 0.011 \times 0.011$ in the lead scintillator and 0.008×0.008 in the lead glass) and also different responses to charged hadrons, which provides important systematic cross-checks for these measurements. A tracking system includes a drift chamber to measure track momentum and pad chamber stations to measure the charged particle hit position [27]. The measurement of the track positions in front of the calorimeter is used to veto charged particles from the photon sample. The beam-beam counters (BBC) are arrays of quartz Čerenkov radiators that surround the beam pipe and are placed ± 144 cm away from the nominal collision point. The BBC covers full azimuth and $3.0 < |\eta| < 3.9$ in pseudorapidity. They measure the z-vertex position; a vertex cut of ± 30 cm around the nominal collision point is used for this analysis. The MB trigger requires at least one charged particle to be measured in both sides of the BBC. This analysis is based on the data sample selected with the EMCal-based high-energy-photon trigger with energy threshold of 1.5 GeV, which is taken in coincidence with the MB trigger.

Photons are identified as clusters in the EMCal and are required to pass a shower profile cut which suppresses clusters from hadrons. High-p_T trigger photons are paired with another photon in the same event that is also on the same side of the detector. A charged track veto cut eliminates clusters that geometrically match with a measured charged track, reducing background from electrons. The contribution of EMCal detector noise is reduced by a minimum energy cut of 0.5 GeV and a time-of-flight cut of $|TOF| < 5$ ns. The timing of the cluster is measured by the EMCal and the time zero reference of the event is provided by the BBC. Each photon pair is required to pass an energy asymmetry cut: $\alpha = |E_1 - E_2|/(E_1 + E_2) < 0.8$. The π^0 yields comprise photon pairs with invariant mass in the signal region ± 25 MeV/c^2 from the π^0 mass peak and η meson yields are measured in the range ± 70 MeV/c^2 around the η mass peak.

The transverse single-spin asymmetries are determined with the "relative luminosity" formula

$$A_N = \frac{1}{P\langle\cos(\phi)\rangle}\frac{N^{\uparrow} - \mathcal{R}N^{\downarrow}}{N^{\uparrow} + \mathcal{R}N^{\downarrow}}, \tag{1}$$

which compares the yield of particles for when the beam was polarized up versus down. Here P is the beam polarization, N refers to the meson yield, the arrows refer to the up ($\uparrow$) or down ($\downarrow$) directions of beam polarization, and $\mathcal{R} = \mathcal{L}^{\uparrow}/\mathcal{L}^{\downarrow}$ is the relative luminosity. The acceptance factor, $\langle\cos(\phi)\rangle$, accounts for the detector azimuthal coverage, where $\phi = 0$ points 90° from the (vertical) spin axis. This correction is calculated as a function of photon pair p_T because the diphoton azimuthal acceptance depends heavily on the decay angle and ranges from 0.95 at low p_T to 0.89 at high p_T. The asymmetry is calculated separately for the two detector arms and then the average weighed by the statistical error is taken for the final result. As written, Eq. (1) is for the arm to the left of the direction of travel of the beam that is being taken as polarized. An overall minus sign is needed for the asymmetry of particle yields in the arm to the right of the polarized-beam-going direction.

An alternative method of calculating the asymmetry is the "square root" formula

$$A_N = \frac{1}{P\langle\cos(\phi)\rangle}\frac{\sqrt{N_L^{\uparrow}N_R^{\downarrow}} - \sqrt{N_L^{\downarrow}N_R^{\uparrow}}}{\sqrt{N_L^{\uparrow}N_R^{\downarrow}} + \sqrt{N_L^{\downarrow}N_R^{\uparrow}}}, \tag{2}$$

which is used as a cross-check. This formula combines data from the two arms (left and right) and both beam polarization directions (up and down). The subscripts in Eq. (2) refer to the yields to the left (L) and right (R) side of the polarized-beam-going direction.

The measured asymmetries are also corrected for background

$$A_N^{\mathrm{Sig}} = \frac{A_N - r \cdot A_N^{\mathrm{BG}}}{1 - r}, \tag{3}$$

where r is the fractional contribution of photon pairs from combinatorial background within the invariant mass peak. The background fraction is calculated from fits to the invariant mass spectra where a Gaussian is used to describe the invariant mass peak, and a third order polynomial is used to describe the combinatorial background, as shown in the green curves in Fig. 1. Using this method, the contribution of combinatorial background under the π^0 peak is determined to vary from 10% in the lowest p_T bin to 6% in the highest. Under the η meson invariant mass peak, the background fraction varies from 71% to 47% in the lowest to highest p_T bins. In Eq. (3), the background asymmetry, A_N^{BG}, is evaluated with photon pairs in sideband regions located on either side of the signal peak, as represented in the red regions in Fig. 1. For the π^0 analysis these sideband regions are $47 < M_{\gamma\gamma} < 97$ MeV/c^2 and

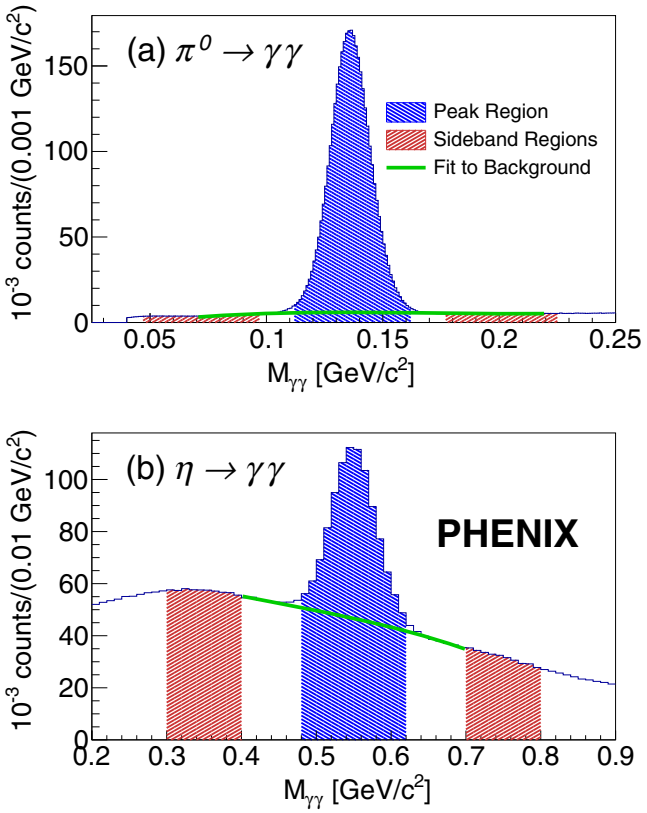

FIG. 1. Example invariant mass distributions around the (a) π^0 and (b) η peak for photon pairs with $4 < p_T < 5$ GeV/c in one of the detector arms. The minus-45° hatched (blue) region at the center of each plot corresponds to the invariant mass region under the peak which is used to calculate A_N in Eq. (3) and the plus-45° (red) sideband regions correspond to the photon pairs that are used to calculate A_N^{BG}. The bold solid (green) curves correspond to the fit to the combinatorial background, which is used to calculate the background fraction.

$177 < M_{\gamma\gamma} < 227$ MeV/c^2, and for the η meson analysis these regions are $300 < M_{\gamma\gamma} < 400$ MeV/c^2 and $700 < M_{\gamma\gamma} < 800$ MeV/c^2. These background regions match the ranges that were used in previous results [5] and are chosen to approximate the behavior of the combinatorial background under the invariant mass peak. They are selected to be close to the peak while still far enough away to contain negligible contributions from signal photon pairs. The background asymmetries are consistent with zero across all p_T bins. The background asymmetries between the low-mass and high-mass regions are also consistent with zero and with each other.

Tables I and II show the asymmetries with statistical and systematic uncertainties. The total systematic uncertainty is the sum of the three sources of systematic uncertainty added in quadrature. The systematic uncertainty on the asymmetry due to the background fraction in Eq. (3) is determined by varying the fit ranges when computing r and calculating how much the background-corrected asymmetry changes. While the asymmetries calculated with the "relative luminosity" [Eq. (1)] and the "square root" [Eq. (2)] formulas were found to be statistically consistent, their difference was assigned as a conservative systematic uncertainty due to possible variations in detector performance and beam conditions. This dominates the total systematic uncertainty for most p_T bins.

Bunch shuffling is a technique used to investigate potential sources of systematic uncertainty that could cause the measured asymmetry results to vary from their true values beyond statistical fluctuations. Bunch shuffling involves randomizing the assigned bunch-by-bunch polarization directions of the beam such that the physical asymmetry disappears, thereby isolating the statistical variations present in the data. All asymmetry values have bunch shuffling results consistent with statistical variations except for the lowest p_T bin where there is 7% and 6% more variation beyond what is expected from statistical fluctuations in the π^0

TABLE I. The measured A_N of π^0 in $p + p$ collisions at $\sqrt{s} = 200$ GeV as a function of p_T. An additional scale uncertainty of 3.4% due to the polarization uncertainty is not shown. The total σ_{syst} in the lowest p_T bin includes an additional systematic uncertainty of 1.06×10^{-4} from bunch shuffling. Columns 5 and 6 show the systematic errors due to relative luminosity vs square root formulas (rel. lumi. vs sqrt.) and background fraction (bg. fraction).

$\langle p_T \rangle$ (GeV/c)	p_T bin ranges (GeV/c)	A_N	σ_{stat}	σ_{syst} (rel. lumi. vs sqrt.)	σ_{syst} (bg. fraction)	σ_{syst} (total)
2.58	2–3	1.43×10^{-4}	2.81×10^{-4}	5.71×10^{-5}	3.92×10^{-7}	1.20×10^{-4}
3.42	3–4	-3.43×10^{-4}	3.21×10^{-4}	1.73×10^{-5}	3.92×10^{-6}	1.77×10^{-5}
4.40	4–5	3.35×10^{-4}	5.71×10^{-4}	6.56×10^{-5}	1.91×10^{-6}	6.57×10^{-5}
5.40	5–6	2.33×10^{-3}	1.06×10^{-3}	9.61×10^{-5}	6.68×10^{-7}	9.61×10^{-5}
6.41	6–7	-6.89×10^{-4}	1.87×10^{-3}	1.12×10^{-4}	2.11×10^{-5}	1.14×10^{-4}
7.42	7–8	1.93×10^{-3}	3.11×10^{-3}	3.41×10^{-4}	7.61×10^{-5}	3.50×10^{-4}
8.43	8–9	-2.38×10^{-3}	4.88×10^{-3}	2.45×10^{-4}	3.99×10^{-4}	4.69×10^{-4}
9.43	9–10	4.04×10^{-4}	7.03×10^{-3}	3.31×10^{-4}	1.16×10^{-4}	3.51×10^{-4}
10.79	10–12	7.34×10^{-3}	7.99×10^{-3}	9.71×10^{-5}	3.13×10^{-4}	3.28×10^{-4}
13.53	10–20	-1.05×10^{-2}	1.27×10^{-2}	6.86×10^{-4}	1.15×10^{-5}	6.86×10^{-4}

TABLE II. The measured A_N of η mesons in $p+p$ collisions at $\sqrt{s}=200$ GeV as a function of p_T. An additional scale uncertainty of 3.4% due to the polarization uncertainty is not shown. The total σ_{syst} in the lowest p_T bin includes an additional systematic uncertainty of 6.20×10^{-4} from bunch shuffling. Columns 5 and 6 show the systematic errors due to relative luminosity vs square root formulas (rel. lumi. vs sqrt.) and background fraction (bg. fraction).

$\langle p_T\rangle$ (GeV/c)	p_T bin ranges (GeV/c)	A_N	σ_{stat}	σ_{syst} (rel. lumi. vs sqrt.)	σ_{syst} (bg. fraction)	σ_{syst} (total)
2.39	2–3	2.44×10^{-3}	1.83×10^{-3}	5.18×10^{-4}	4.58×10^{-5}	8.09×10^{-4}
3.53	3–4	-1.99×10^{-3}	1.59×10^{-3}	8.36×10^{-5}	3.31×10^{-5}	8.99×10^{-5}
4.39	4–5	-3.31×10^{-3}	2.48×10^{-3}	1.44×10^{-4}	4.55×10^{-5}	1.51×10^{-4}
5.40	5–6	-1.39×10^{-3}	4.21×10^{-3}	2.41×10^{-4}	3.59×10^{-5}	2.44×10^{-4}
6.41	6–7	2.22×10^{-3}	7.09×10^{-3}	1.12×10^{-3}	6.35×10^{-6}	1.12×10^{-3}
7.42	7–8	1.03×10^{-2}	1.15×10^{-2}	7.03×10^{-4}	1.60×10^{-4}	7.20×10^{-4}
8.75	8–10	7.90×10^{-3}	1.37×10^{-2}	1.24×10^{-3}	1.88×10^{-4}	1.25×10^{-3}
11.76	10–20	1.68×10^{-2}	2.19×10^{-2}	4.25×10^{-3}	3.70×10^{-4}	4.26×10^{-3}

and η meson analyses, respectively. These values are used to assign additional systematic uncertainties to the lowest p_T bin of the π^0 and η meson asymmetries and dominate the total systematic uncertainty for those bins.

Additional cross-checks included examining the asymmetries in the two arms separately using Eq. (1) and measuring the asymmetry as an explicit function of ϕ. All checks were statistically consistent with the main asymmetry results.

III. RESULTS AND DISCUSSION

Figure 2 shows the A_N of neutral pions at midrapidity in $p^\uparrow+p$ collisions at $\sqrt{s}=200$ GeV, where the bands represent the systematic uncertainty and the bars represent the statistical uncertainty. The comparison to previous results [5] demonstrates the improvement in statistical precision. The inset in Fig. 2 shows a zoomed-in comparison at small p_T. The new measurement is consistent with our previous measurement and improves the precision on average by a factor of 3. The new measurement of A_N of neutral pions is consistent with zero in the entire p_T range.

The measurement of A_N of η mesons in $p^\uparrow+p$ collisions at $\sqrt{s}=200$ GeV is shown in Fig. 3. This measurement is also compared to the previous result, similarly to Fig. 2. The new measurement is consistent with the previous result and with zero across the entire p_T range. In principle, comparisons of π^0 and η meson TSSAs may indicate additional effects from strange quarks, isospin differences, or hadron mass. At forward rapidity, existing measurements [22,28] do not yet clearly resolve whether the η meson asymmetry is larger than the π^0 asymmetry as predicted in some models [29]. At midrapidity, there is a larger contribution from gluon dynamics and, as shown in Fig. 4, both asymmetries are consistent with zero and therefore show no evidence for differences due to strangeness, isospin, or mass.

Figure 5 shows this π^0 TSSA result plotted with theoretical predictions. The qgq curve shows the predicted contribution from collinear twist-3 qgq functions from both the polarized proton and the process of hadronization. This curve was calculated with fits that were published in Ref. [10] and has been reevaluated in the rapidity range of PHENIX. Midrapidity π^0 production includes a large

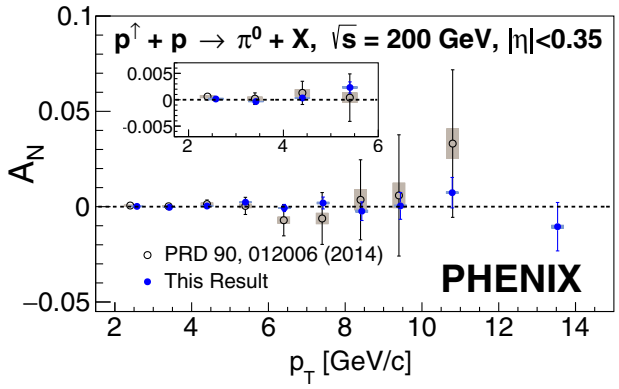

FIG. 2. Transverse single-spin asymmetry of neutral pions measured at $|\eta|<0.35$ in $p^\uparrow+p$ collisions at $\sqrt{s}=200$ GeV. An additional scale uncertainty of 3.4% due to the polarization uncertainty is not shown.

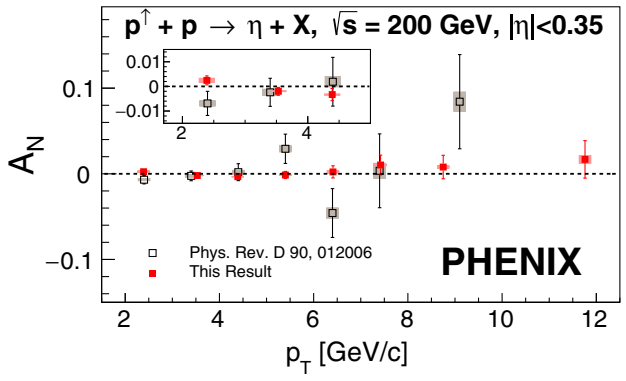

FIG. 3. Transverse single-spin asymmetry of eta mesons measured at $|\eta|<0.35$ in $p^\uparrow+p$ collisions at $\sqrt{s}=200$ GeV. An additional scale uncertainty of 3.4% due to the polarization uncertainty is not shown.

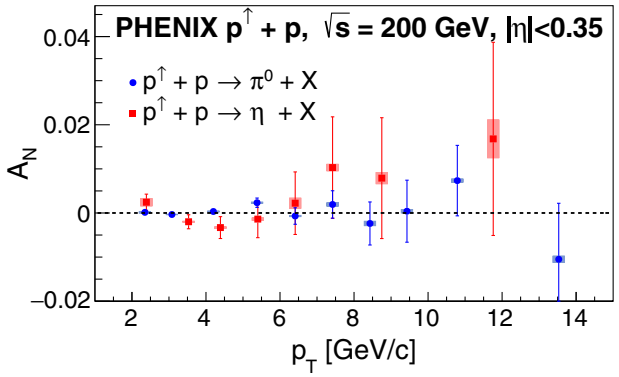

FIG. 4. Comparison of the π^0 and η meson asymmetries measured at $|\eta| < 0.35$ in $p^{\uparrow} + p$ collisions at $\sqrt{s} = 200$ GeV. An additional scale uncertainty of 3.4% due to the polarization uncertainty is not shown.

fractional contribution from gluons in the proton, so a complete collinear twist-3 description of the midrapidity π^0 TSSA would also need to include the contribution from the trigluon correlation function. Given the small expected contribution from the qgq correlation function, this measurement can constrain future calculations of the ggg correlation function, such as those in Ref. [30].

The other theory curves in Fig. 5 show predictions for the midrapidity π^0 TSSA generated by the Sivers TMD PDF. These curves include contributions from both the quark and gluon Sivers functions and have been evaluated for $x_F = 0$, which approximates the measured kinematics. These calculations use the generalized parton model (GPM) which takes the first k_T moment of the Sivers function [e.g., $\int k_T \cdot q(k_T)$] and does not include next-to-leading-order interactions with the proton fragments. The "GPM" curve uses the parameters stated in Eq. (32) of Ref. [31]. The color-gauge-invariant generalized parton model (CGI-GPM) expands on the GPM by including initial- and final-state interactions through the one-gluon exchange

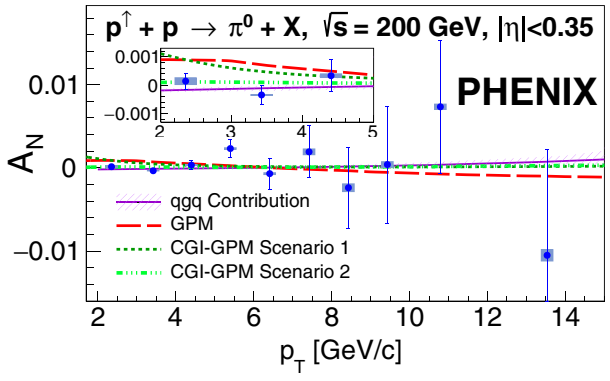

FIG. 5. This π^0 asymmetry result plotted with theory calculations for the asymmetry in both the collinear twist-3 [10] and TMD [31] theoretical frameworks. See text for details.

approximation. This model has been shown to reproduce the predicted sign change for the quark Sivers function in SIDIS and Drell-Yan. The CGI-GPM curves plotted in Fig. 5 show two different scenarios for this model, the specifics of which can be found in Eq. (34) of Ref. [31]. The values that are used for the scenario 1 curve are chosen to maximize the open heavy flavor TSSA generated by the gluon Sivers function while still keeping this asymmetry within the statistical error bars of the published result in Ref. [32] and simultaneously describing the previously published midrapidity π^0 TSSA from Ref. [5]. The values used in the scenario 2 curve are similarly calculated, except that they minimize the open heavy flavor TSSA within the range of the published statistical error bars. As shown in the zoomed-in inset of Fig. 5, this π^0 TSSA result has the statistical precision at low p_T needed to distinguish between the GPM and CGI-GPM frameworks, preferring CGI-GPM scenario 2.

Measurements of TSSAs in $p + p$ collisions are essential to understanding the underlying nonperturbative processes which generate them. In particular, further measurements are necessary to clarify certain questions in the interpretations of the TSSAs. For example, the small forward jet asymmetries measured in Ref. [20] have been interpreted as a cancellation of up and down quark asymmetries, implying that the comparatively forward large neutral pion asymmetries include significant contributions from spin-momentum correlations in hadronization [19]. Additionally, the p_T dependence of these forward rapidity measurements remains to be clearly understood; measurements of nonzero asymmetries out to even higher p_T would help confirm that these twist-3 observables eventually fall off with increasing hard scale. While the midrapidity measurements here are all consistent with zero, they still provide the highest available statistical precision and p_T reach available at the PHENIX experiment. While forward rapidity light hadron TSSAs are dominated by valence quark spin-momentum correlations in the polarized proton, these midrapidity TSSA measurements are sensitive to both quark and gluon dynamics at leading order. Thus these data also provide further constraints to gluon spin-momentum correlations in transversely polarized protons [30,33].

IV. SUMMARY

The measurements presented here were motivated by the outstanding questions regarding the physical origin of TSSAs. The TSSAs of π^0 and η mesons were measured at midrapidity in $p + p$ collisions at $\sqrt{s} = 200$ GeV by the PHENIX experiment. The measured π^0 (η) meson asymmetry is consistent with zero in the presented p_T range, up to precision of 3×10^{-4} (2×10^{-3}) in the lowest p_T bins. Both measurements have a significant reduction in uncertainty from previous measurements at midrapidity at RHIC.

These data extend previous constraints to any presence of gluon spin-momentum correlations in transversely polarized protons.

ACKNOWLEDGMENTS

We thank the staff of the Collider-Accelerator and Physics Departments at Brookhaven National Laboratory and the staff of the other PHENIX participating institutions for their vital contributions. We also thank D. Pitonyak, S. Yoshida, U. D'Alesio, F. Murgia and C. Pisano for helpful discussions. We acknowledge support from the Office of Nuclear Physics in the Office of Science of the Department of Energy, the National Science Foundation, Abilene Christian University Research Council, Research Foundation of SUNY, and Dean of the College of Arts and Sciences, Vanderbilt University (U.S.A.), Ministry of Education, Culture, Sports, Science, and Technology and the Japan Society for the Promotion of Science (Japan), Conselho Nacional de Desenvolvimento Científico e Tecnológico and Fundação de Amparo à Pesquisa do Estado de São Paulo (Brazil), Natural Science Foundation of China (People's Republic of China), Croatian Science Foundation and Ministry of Science and Education (Croatia), Ministry of Education, Youth and Sports (Czech Republic), Centre National de la Recherche Scientifique, Commissariat à l'Énergie Atomique, and Institut National de Physique Nucléaire et de Physique des Particules (France), Bundesministerium für Bildung und Forschung, Deutscher Akademischer Austausch Dienst, and Alexander von Humboldt Stiftung (Germany), J. Bolyai Research Scholarship, EFOP, the New National Excellence Program (ÚNKP), NKFIH, and OTKA (Hungary), Department of Atomic Energy and Department of Science and Technology (India), Israel Science Foundation (Israel), Basic Science Research and SRC(CENuM) Programs through NRF funded by the Ministry of Education and the Ministry of Science and ICT (Korea), Physics Department, Lahore University of Management Sciences (Pakistan), Ministry of Education and Science, Russian Academy of Sciences, Federal Agency of Atomic Energy (Russia), VR and Wallenberg Foundation (Sweden), the U.S. Civilian Research and Development Foundation for the Independent States of the Former Soviet Union, the Hungarian American Enterprise Scholarship Fund, the U.S.-Hungarian Fulbright Foundation, and the U.S.-Israel Binational Science Foundation.

[1] R. D. Klem, J. E. Bowers, H. W. Courant, H. Kagan, M. L. Marshak, E. A. Peterson, K. Ruddick, W. H. Dragoset, and J. B. Roberts, Measurement of Asymmetries of Inclusive Pion Production in Proton Proton Interactions at 6-GeV/c and 11.8-GeV/c, Phys. Rev. Lett. **36**, 929 (1976).

[2] D. L. Adams *et al.* (FNAL-E704 Collaboration), Analyzing power in inclusive π^+ and π^- production at high x_F with a 200-GeV polarized proton beam, Phys. Lett. B **264**, 462 (1991).

[3] B. I. Abelev *et al.* (STAR Collaboration), Forward Neutral Pion Transverse Single Spin Asymmetries in $p+p$ Collisions at $\sqrt{s}=200$ GeV, Phys. Rev. Lett. **101**, 222001 (2008).

[4] I. Arsene *et al.* (BRAHMS Collaboration), Single Transverse Spin Asymmetries of Identified Charged Hadrons in Polarized $p+p$ Collisions at $\sqrt{s}=62.4$ GeV, Phys. Rev. Lett. **101**, 042001 (2008).

[5] A. Adare *et al.* (PHENIX Collaboration), Measurement of transverse-single-spin asymmetries for midrapidity and forward-rapidity production of hadrons in polarized $p+p$ collisions at $\sqrt{s}=200$ and 62.4 GeV, Phys. Rev. D **90**, 012006 (2014).

[6] J. Adam *et al.* (STAR Collaboration), Measurement of transverse single-spin asymmetries of π^0 and electromagnetic jets at forward rapidity in 200 and 500 GeV transversely polarized proton-proton collisions, arXiv:2012.11428.

[7] G. L. Kane, J. Pumplin, and W. Repko, Transverse Quark Polarization in Large p_T Reactions, e^+e^- Jets, and Leptoproduction: A Test of QCD, Phys. Rev. Lett. **41**, 1689 (1978).

[8] D. W. Sivers, Single spin production asymmetries from the hard scattering of pointlike constituents, Phys. Rev. D **41**, 83 (1990).

[9] J. C. Collins, Fragmentation of transversely polarized quarks probed in transverse momentum distributions, Nucl. Phys. **B396**, 161 (1993).

[10] J. Cammarota, L. Gamberg, Z.-B. Kang, J. A. Miller, D. Pitonyak, A. Prokudin, T. C. Rogers, and N. Sato (Jefferson Lab Angular Momentum Collaboration), Origin of single transverse-spin asymmetries in high-energy collisions, Phys. Rev. D **102**, 054002 (2020).

[11] S. M. Aybat, J. C. Collins, J. W. Qiu, and T. C. Rogers, The QCD evolution of the Sivers function, Phys. Rev. D **85**, 034043 (2012).

[12] X. Ji, J. W. Qiu, W. Vogelsang, and F. Yuan, A Unified Picture for Single Transverse-Spin Asymmetries in Hard Processes, Phys. Rev. Lett. **97**, 082002 (2006).

[13] J. C. Collins, Leading twist single transverse-spin asymmetries: Drell-Yan and deep inelastic scattering, Phys. Lett. B **536**, 43 (2002).

[14] A. Airapetian *et al.* (HERMES Collaboration), Single-Spin Asymmetries in Semi-Inclusive Deep-Inelastic Scattering on a Transversely Polarized Hydrogen Target, Phys. Rev. Lett. **94**, 012002 (2005).

[15] C. Adolph *et al.* (COMPASS Collaboration), Collins and Sivers asymmetries in muonproduction of pions and kaons off transversely polarised protons, Phys. Lett. B **744**, 250 (2015).

[16] T. C. Rogers and P. J. Mulders, No generalized TMD factorization in hadroproduction of high transverse momentum hadrons, Phys. Rev. D **81**, 094006 (2010).
[17] T. C. Rogers, Extra spin asymmetries from the breakdown of transverse-momentum-dependent factorization in hadron-hadron collisions, Phys. Rev. D **88**, 014002 (2013).
[18] J. Adam *et al.* (STAR Collaboration), Comparison of transverse single-spin asymmetries for forward π^0 production in polarized pp, pAl and pAu collisions at nucleon pair c.m. energy $\sqrt{s_{\rm NN}} = 200$ GeV, arXiv:2012.07146.
[19] K. Kanazawa, Y. Koike, A. Metz, and D. Pitonyak, Towards an explanation of transverse single-spin asymmetries in proton-proton collisions: The role of fragmentation in collinear factorization, Phys. Rev. D **89**, 111501 (2014).
[20] L. C. Bland *et al.* (AnDY Collaboration), Cross sections and transverse single-spin asymmetries in forward jet production from proton collisions at $\sqrt{s} = 500$ GeV, Phys. Lett. B **750**, 660 (2015).
[21] J. H. Lee and F. Videbaek (for the BRAHMS Collaboration), Cross sections and single spin asymmetries of identified hadrons in $p^\uparrow + p$ at $\sqrt{s} = 200$ GeV, in Proceedings of the XVII International Workshop on Deep-Inelastic Scattering and Related Topics (Madrid, Spain, 2009) [arXiv:0908.4551].
[22] A. Adare *et al.* (PHENIX Collaboration), Cross section and transverse single-spin asymmetry of η mesons in $p^\uparrow + p$ collisions at $\sqrt{s} = 200$ GeV at forward rapidity, Phys. Rev. D **90**, 072008 (2014).
[23] L. Adamczyk *et al.* (STAR Collaboration), Observation of Transverse Spin-Dependent Azimuthal Correlations of Charged Pion Pairs in $p^\uparrow + p$ at $\sqrt{s} = 200$ GeV, Phys. Rev. Lett. **115**, 242501 (2015).
[24] L. Adamczyk *et al.* (STAR Collaboration), Transverse spin-dependent azimuthal correlations of charged pion pairs measured in $p^\uparrow + p$ collisions at $\sqrt{s} = 500$ GeV, Phys. Lett. B **780**, 332 (2018).
[25] W. D. Schmidke *et al.* (The RHIC Polarimetry Group), RHIC polarization for runs 9–17, Report No. BNL-209057-2018-TECH, 2018.
[26] L. Aphecetche *et al.* (PHENIX Collaboration), PHENIX calorimeter, Nucl. Instrum. Methods Phys. Res., Sect. A **499**, 521 (2003).
[27] K. Adcox *et al.* (PHENIX Collaboration), PHENIX central arm tracking detectors, Nucl. Instrum. Methods Phys. Res., Sect. A **499**, 489 (2003).
[28] L. Adamczyk *et al.* (STAR Collaboration), Transverse single-spin asymmetry and cross-section for π^0 and η mesons at large Feynman-x in polarized $p + p$ collisions at $\sqrt{s} = 200$ GeV, Phys. Rev. D **86**, 051101 (2012).
[29] K. Kanazawa and Y. Koike, A phenomenological study on single transverse-spin asymmetry for inclusive light-hadron productions at RHIC, Phys. Rev. D **83**, 114024 (2011).
[30] H. Beppu, K. Kanazawa, Y. Koike, and S. Yoshida, Three-gluon contribution to the single spin asymmetry for light hadron production in pp collision, Phys. Rev. D **89**, 034029 (2014).
[31] U. D'Alesio, C. Flore, F. Murgia, C. Pisano, and P. Taels, Unraveling the gluon Sivers function in hadronic collisions at RHIC, Phys. Rev. D **99**, 036013 (2019).
[32] C. Aidala *et al.* (PHENIX Collaboration), Cross section and transverse single-spin asymmetry of muons from open heavy-flavor decays in polarized $p + p$ collisions at $\sqrt{s} = 200$ GeV, Phys. Rev. D **95**, 112001 (2017).
[33] U. D'Alesio, F. Murgia, and C. Pisano, Towards a first estimate of the gluon Sivers function from A_N data in pp collisions at RHIC, J. High Energy Phys. 09 (2015) 119.